

See discussions, stats, and author profiles for this publication at: <https://www.researchgate.net/publication/243374720>

Density Functional Theory Study of the Adsorption and Reaction of H₂S on TiO₂ Rutile (110) and Anatase (101) Surfaces

ARTICLE *in* THE JOURNAL OF PHYSICAL CHEMISTRY C · NOVEMBER 2009

Impact Factor: 4.77 · DOI: 10.1021/jp906948a

CITATIONS

25

READS

124

3 AUTHORS, INCLUDING:



[Hsin-Tsung Chen](#)

Chung Yuan Christian University

78 PUBLICATIONS 703 CITATIONS

[SEE PROFILE](#)

Density Functional Theory Study of the Adsorption and Reaction of H₂S on TiO₂ Rutile (110) and Anatase (101) Surfaces

Wen-Fei Huang,[†] Hsin-Tsung Chen,^{*,‡} and M. C. Lin^{*,†,§}

Institute of Molecular Science, National Chiao Tung University, Hsinchu, Taiwan 300, National Center for High-performance Computing, No. 28, Nan-Ke 3rd Road, Hsin-Shi, Tainan, 74147, Taiwan, and Department of Chemistry, Emory University, Atlanta, Georgia 30322

Received: July 22, 2009; Revised Manuscript Received: September 14, 2009

The adsorption and reaction of H₂S on TiO₂ rutile (110) and anatase (101) surfaces have been investigated by using periodic density functional theory (DFT) in conjunction with the projected augmented wave (PAW) approach. Adsorption mechanisms of H₂S, HS, and S on both surfaces were analyzed. It was found that H₂S, HS, S, and H preferentially adsorb at the Ti_{5c}, O_{2c}, (Ti_{5c})₂, and O_{2c} sites, respectively, on the rutile surface, and at the Ti_{5c}, (Ti_{5c})₂, (−O_{2c})−(−Ti_{5c}), and O_{2c} sites, respectively, on the anatase surface. Potential energy profiles of the adsorption processes on both surfaces producing H₂ and H₂O were constructed using the nudged elastic band (NEB) method. Forming surface sulfur species by a complete O ↔ S exchange at the rutile surface is endothermic by 15.4 kcal/mol and requires a high energy barrier of 35.5 kcal/mol, while it is endothermic by 5.0 kcal/mol and requires a lower energy barrier of 12.4 kcal/mol at the anatase surface. The rate constants for the dehydrogenation and dehydration processes have been predicted.

I. Introduction

Titanium dioxide has become attractive recently in numerous theoretical and experimental studies because of its promising photoelectrochemical and photocatalytic applications.^{1,2} Fujishima and Honda studied the photoelectrochemical splitting of H₂O on the TiO₂ rutile surface in the early 1970s.³ Elucidation of the small molecule–TiO₂ surface interaction mechanisms continues to be of interest to numerous investigations.^{4–10} It was found that doping with nonmetal elements (S, N, C, B, P, F)^{5,11–19} could efficiently extend its optical absorption edge into the visible light region and enhance its photocatalytic activity. For example, N-doped TiO₂ (TiO_{2-x}N_x) had been shown to make the TiO₂ band gap lower evidently by the mixing of nitrogen p states and oxygen 2p states.^{5,20–22} Liu et al.²² have reported that the band gap can be reduced with an increasing amount of S in the S-doped TiO₂. Experimentally, the S-doped TiO₂ also shows a strong absorbance for the visible light.^{23,24} However, little work has been done to account for the mechanism for the formation of S-doped TiO₂.

Many studies on the interaction of H₂S and its fragments on TiO₂ surfaces,^{25,26} metal oxide,^{27–29} or metal^{30–34} have been reported. Smith et al. annealed TiO₂ with TiS₂ to obtain the S-doped TiO₂,²³ and Chen et al. used H₂S as a precursor to produce a S-doped TiO₂ surface.²⁴ To our best knowledge, the mechanisms for these processes are not clear. Possible pathways of the H₂S molecule adsorbed on TiO₂ have been reported by Chen et al.²⁴ It was shown that the adsorption of H₂S on the TiO₂ surface occurs via the dissociative pathways, H₂S → HS + H and HS → S + H, to produce H₂O and O vacancies. Then, S may move into the O vacancy, forming the S-doped TiO₂ surface. The TiO₂ nanoparticle film is a polycrystalline material with different phases. The rutile (110) and anatase (101)

surfaces, which have the lowest surface energies with similar characteristics, may coexist in a nanoparticle film.³⁵ Theoretically, the (110) and (101) are the most stable surfaces in the rutile and anatase, respectively, as reported by Labat et al.³⁶ Therefore, in this work, we attempt to elucidate the interaction and the mechanism for the H₂S on the TiO₂ surfaces by density functional theory (DFT). The adsorption geometries and energies of H₂S and its fragments, HS, H, and S, on both surfaces have been completed. In addition, the reaction rate constants for key processes involved have been calculated based on the potential energy surface (PES) for H₂S on both surfaces.

II. Computational Methods and Models

Reactants, intermediates, transition states, and products of the reactions of H₂S and its fragments on both surfaces were calculated at the DFT plane-wave level utilizing the Vienna ab initio simulation package (VASP)^{37,38} with the projected augmented wave method (PAW).³⁹ The generalized gradient approximation (GGA) with the Perdew–Wang 1991 (PW91)⁴⁰ formulation, which has been shown to work well for surfaces,^{41,42} was used in these calculations. These plane-wave expansions included all plane waves with their kinetic energies smaller than the chosen cutoff energy, $\hbar k^2/2m < E_{\text{cut}}$, which ensures the convergence with respect to the basis set. The Brillouin zone was sampled with the chosen Monkhorst–Pack k -points, which also ensure the convergence of the calculation. The calculations were carried out with the (2 × 4 × 2) and (4 × 4 × 1) Monkhorst–Pack k -points using a 500 eV cutoff energy for the rutile bulk and (110) surfaces, while the (4 × 4 × 4) and (6 × 4 × 1) Monkhorst–Pack k -points with the same cutoff energy were chosen for the anatase bulk and (101) surfaces, respectively. Spin polarization was considered for the radicals in these calculations. It should be mentioned that we have also performed calculations for H₂S, HS, and S adsorption on larger surfaces for two phases, corresponding to coverages of 1/4, 1/3, and 1/6 ML, respectively, using the most stable configurations. It was shown that the coverage effect is negligible due to the relative

* Corresponding authors. E-mail: htchen@nchc.org.tw and chemmcl@emory.edu.

[†] National Chiao Tung University.

[‡] National Center for High-performance Computing.

[§] Emory University.

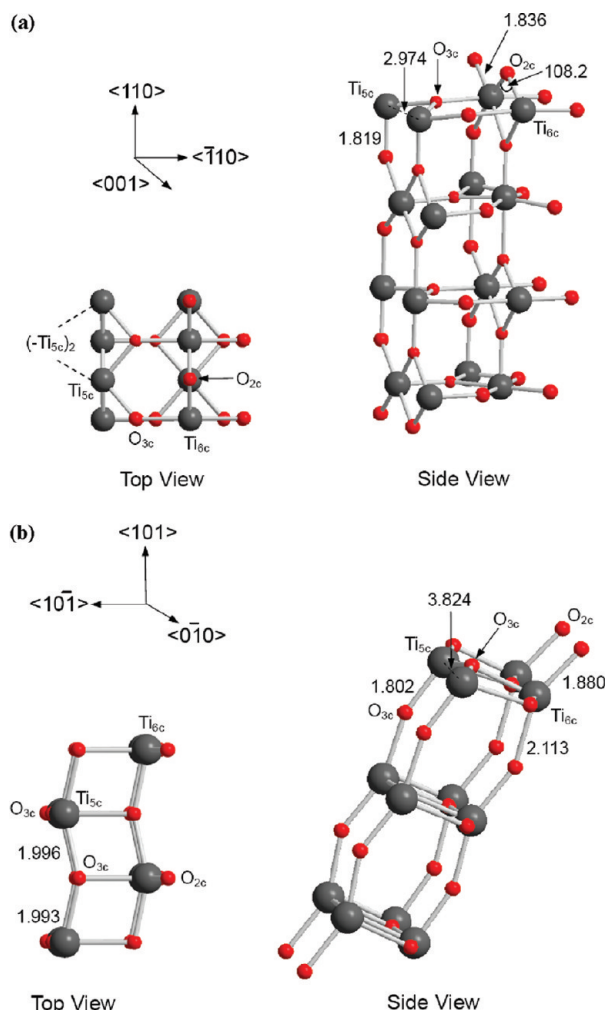


Figure 1. The geometries of the optimized TiO_2 rutile (110) and the TiO_2 anatase (101) surfaces: (a) rutile (110) surface; (b) anatase (101) surface. The bond lengths and angles are in angstroms and degrees, respectively.

energy smaller than 1.0 kcal/mol. Therefore, in the present study, we only use the computationally less expensive model of both surfaces.

The rutile and anatase surfaces were modeled as periodically repeated slabs consisting of 16 and 12 $[\text{TiO}_2]$ unit cells, respectively, as shown in Figure 1a and b. All slabs were separated by a vacuum spacing of about 20 Å, which guaranteed no interactions between the slabs. The lower layers were fixed to set the estimated bulk parameters, while the remaining layers were fully relaxed during the calculations. The adsorption energies were calculated by the following equation:

$$E_{\text{ads}} = -(E_{\text{total}} - E_{\text{surf}} - E_{\text{gas}})$$

where E_{total} , E_{surf} , and E_{gas} are the calculated electronic energies of the adsorbed species on the surface, a clean surface, and a gas-phase molecule, respectively. The nudged elastic band (NEB) method^{43,44} was applied to locate the transition states (TSs). Two to eight images were used for each calculated TS. All transition structures were verified by the frequency calculations. The rate constants were calculated by the microcanonical Rice–Ramsperger–Kassel–Marcus (RRKM) theory using the ChemRate program.⁴⁵ Charge analyses of the optimized structures were carried out by utilizing the Bader atomic charge method.⁴⁶

TABLE 1: Geometrical Parameters of H_2S and HS Molecules

	H–S bond length (Å)			H–S–H angle (deg)		
	this work	expt.	calc.	this work	expt.	calc.
H_2S	1.346	1.328 ⁴⁹	1.349, ²⁸ 1.35 ³²	91.7	92.2 ⁴⁵	91.6, ²⁸ 92.1 ³²
HS	1.351	1.345 ⁴⁵	1.354, ²⁸ 1.355 ³²			

III. Results and Discussion

To ensure the reliability of the computational results, we first compared the calculated bulk lattice constants. The predicted lattice constants are $a = 4.593$ Å and $c = 2.958$ Å for rutile, which are in good agreement with the experimental values⁴⁷ of $a = 4.587\text{--}4.593$ Å and $c = 2.954\text{--}2.959$ Å, while those for anatase are $a = 3.824$ Å and $c = 9.678$ Å which are in reasonable agreement with the experimental values^{47,48} of $a = 3.782\text{--}3.785$ Å and $c = 9.502\text{--}9.514$ Å. As summarized in Table 1, the calculated geometrical parameters of H_2S and HS in a 10 Å cubic box are also in line with the experimental⁴⁹ and theoretical^{30,34} values. The reaction energy (ΔE) of $\text{H}_2\text{S}_{(\text{g})} \rightarrow \text{HS}_{(\text{g})} + \text{H}_{(\text{g})}$ was calculated to be 94.2 kcal/mol, which is consistent with the experimental and theoretical values of 95.5⁴⁹ and 96.7³⁰ kcal/mol, respectively.

In general, the H_2S molecule, as well as its fragments, HS, S, and H, can adsorb on both TiO_2 surfaces via several ways. Shown in Figure 1, four different adsorption sites on both surfaces have been labeled. They are 5-fold coordinated titanium, 6-fold coordinated titanium, 2-fold bridging oxygen, and 3-fold coordinated oxygen, corresponding to Ti_{5c} , Ti_{6c} , O_{2c} , and O_{3c} , respectively.

III.1. Adsorption and Reaction of H_2S on the TiO_2 Surface. III.1.1. Adsorption of H_2S , HS, S, and H on the Rutile (110) Surface.

H_2S Adsorption. H_2S molecule can interact with the TiO_2 rutile (110) surface via several different ways by utilizing its H atoms and S lone-pair electrons. On the TiO_2 (110) surface, the Ti_{5c} and O_{2c} sites are more active than the Ti_{6c} and O_{3c} sites due to their unsaturated coordinations, which are evidenced by previous theoretical studies.⁹ Here, we discuss only energetically more favorable structures, $\text{H}_2\text{S}-\text{Ti}_{5c}(\text{a})$, $\text{H}_2\text{S}-\text{O}_{2c}(\text{a})$, $\text{H}_2\text{S}-\text{(Ti}_{5c}\text{)}_2(\text{a})$, $\text{HSH}-\text{Ti}_{5c}(\text{a})$, $\text{HSH}-\text{O}_{2c}(\text{a})$, and $\text{O}_{2c}-\text{HSH}-\text{O}_{2c}(\text{a})$, as shown in Figure 2 and Figure S1 of the Supporting Information (the most stable adsorption geometry is shown in Figure 2, and the remains are displayed in Figure S1). As summarized in Table 2, the calculated adsorption energies for these configurations are 12.9, 2.3, 3.5, 1.3, 3.0, and 4.2 kcal/mol, respectively. The $\text{H}_2\text{S}-\text{Ti}_{5c}(\text{a})$ configuration is the most stable, indicating that H_2S prefers to interact with Ti_{5c} through its lone-pair electrons, similar to the previous studies on H_2O rutile (110) TiO_2 interactions reported by Harris et al.⁹ and Lindan et al.⁴³ In $\text{H}_2\text{S}-\text{Ti}_{5c}(\text{a})$, the H–S bond length of H_2S is 1.373 Å, which is 0.027 Å longer than that in the gas phase due to the formation of the S–Ti bond and the H··· O_{2c} hydrogen bonding. The H··· O_{2c} distance is 1.890 Å, and the S– Ti_{5c} bond length is 2.757 Å, which is the shortest distance between the adsorbate molecule and the surface in these adsorption structures. The $\text{H}_2\text{S}-\text{O}_{2c}(\text{a})$, $\text{H}_2\text{S}-\text{(Ti}_{5c}\text{)}_2(\text{a})$, $\text{HSH}-\text{Ti}_{5c}(\text{a})$, $\text{HSH}-\text{O}_{2c}(\text{a})$, and $\text{O}_{2c}-\text{HSH}-\text{O}_{2c}(\text{a})$ structures can be characterized as physisorbed species with small adsorption energies and long distances between the H_2S molecule and the surface, 3.197, 4.011, 2.808, 2.515, and 2.211 Å, respectively.

HS, S, and H Adsorption. In order to carry out mechanistic studies, we examined the adsorption sites and energies for HS, S, and H on rutile TiO_2 (110) as well. Figure 2 displays the most stable optimized local minimum of the HS species on the

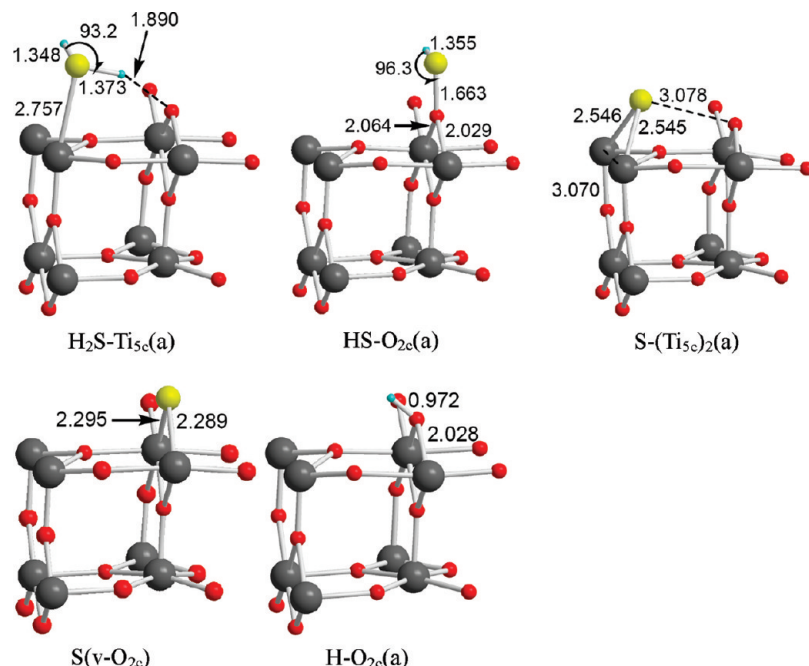


Figure 2. Optimized geometries of adsorbed H₂S and its fragments, HS, S, and H, on the TiO₂ rutile (110) surface. The bond lengths and angles are in angstroms and degrees, respectively.

TABLE 2: Adsorption Energies (kcal/mol) of H₂S, HS, and S Species on TiO₂ Rutile (110) and TiO₂ Anatase (101) Surfaces

		H ₂ S	HSH	HS	S	S,O _{2c} (v)	H-
on rutile	-Ti _{5c}	12.9	1.3	12.2	15.2	50.1	1.6
	-O _{2c}	2.3	3.0	18.7	28.8	90.0 ^b	63.5
	-(Ti _{5c}) ₂	3.5	4.2 ^a	9.4	38.6	43.8	
on anatase	-Ti _{5c}	11.4	<i>d</i>	11.1	11.8	61.1	0.3
	-O _{2c}	1.1	3.2	9.8	46.5 ^e	115.9 ^b	55.4
	-(Ti _{5c}) ₂	<i>d</i>	2.5 ^a	11.5 ^c	33.2	<i>d</i>	

^a O_{2c}-HSH-O_{2c}(a). ^b S in the oxygen vacancy site, S(v-O_{2c}). ^c HS(-Ti_{5c})(-O_{3c}). ^d Unstable. ^e S(-O_{2c})(-Ti_{5c}).

surface, while other possible structures are depicted in Figure S1 of the Supporting Information. Their adsorption energies are summarized in Table 2. While H₂S preferentially adsorbs on the Ti_{5c} site, the most stable configuration for HS adsorption is located at the O_{2c} bridging site. For the **HS-O_{2c}(a)** structure with adsorption energies of 18.7 kcal/mol, the S atom is bound to an O anion of the surface with a S–O distance of 1.663 Å. Due to the strong overlap between p orbitals of the S atom and the surface O anion, the S–O covalent bond results in a higher adsorption energy. In addition, the formation of the S–O bond produces much relaxation of the surface O anion bonded to the sulfur atom, resulting in the protrusion by approximately 0.2 Å from the surface. The adsorption energy of **HS-Ti_{5c}(a)** is 12.2 kcal/mol, and the Ti_{5c}–S bond length (2.642 Å) is slightly shorter than that of **H₂S-Ti_{5c}(a)** for H₂S adsorption (2.757 Å).

For S adsorption, the S atom is favorably placed on two 5-fold Ti sites (Ti_{5c})₂, as shown in Figure 2. Table 2 shows that **S-(Ti_{5c})₂** with an adsorption energy of 38.6 kcal/mol is the most stable, while **S-Ti_{5c}(a)** and **S-O_{2c}(a)** (see Figure S1 of the Supporting Information) have energies of 15.2 and 28.8 kcal/mol, respectively. The Ti–S distances of **S-Ti_{5c}** and **S-(Ti_{5c})₂** are 2.562 and 2.546 Å, respectively, while the S–O distance of **S-O_{2c}** is 1.659 Å. Similar to the HS adsorption, the surface O anion bonded to the sulfur atom moves upward by approximately 0.2 Å. In addition, we also considered the adsorption of S on a reduced TiO₂ surface, on which one of the

bridging site O_{2c} atoms was removed, resulting in an O vacancy due to product desorption. As presented in Figure 2, the S atom is favorably adsorbed on an O vacant site with an absorption energy of 90.0 kcal/mol. Other less stable structures are displayed in Figure S1 of the Supporting Information. The distance of S–Ti_{6c} in **S(v-O_{2c})** is 0.45 Å longer than the distance of O_{2c}–Ti_{6c} on the TiO₂ surface, because the S–Ti bond is weaker than the O–Ti bond due to the larger S atom. The adsorption energies and structures of H₂S, HS, and S are all in close agreement with similar adsorption on TiO, Al₈O₁₂, Al₆O₉, Cr₈O₁₂, and Cr₆O₉.^{25,26,28}

Regarding H adsorption, we optimized two configurations on the Ti_{5c} and O_{2c} sites. Similar to recent theoretical results by Wang and Lin,⁶ the H atom adsorbs preferentially on the O_{2c} site with an absorption energy and O–H distance of 63.5 kcal/mol and 0.972 Å, respectively, while the adsorption energy of H–Ti_{5c}(a) is only 1.6 kcal/mol.

III.1.2. Adsorption of H₂S, HS, S, and H on the Anatase (101) Surface. **H₂S Adsorption.** Only four energetically more favorable structures, **H₂S-Ti_{5c}(a)**, **H₂S-O_{2c}(a)**, **HSH-O_{2c}(a)**, and **O_{2c}-HSH-O_{2c}(a)**, were found (see Figure 3 and Figure S2 of the Supporting Information; the most stable adsorption geometry is shown in Figure 3, and the less stable ones are displayed in Figure S2). Their calculated adsorption energies are 11.4, 1.1, 3.2, and 2.5 kcal/mol (see Table 2), respectively. The most stable configuration is **H₂S-Ti_{5c}(a)**, which adsorbs on Ti_{5c} through its lone-pair electrons similar to that on the rutile (110) surface and H₂O^{50,51} on the anatase (101) surface. The bond lengths of H···O_{2c} (2.322 Å) and S–Ti_{5c} (2.828 Å) are somehow longer than those on the rutile (110) surface. The **H₂S-O_{2c}(a)**, **HSH-O_{2c}(a)**, and **O_{2c}-HSH-O_{2c}(a)** structures can be characterized as physisorbed species with small adsorption energies and long distances between the H₂S molecule and the surface, 3.008, 2.561, 2.276, and 2.245 Å, respectively. The H₂S adsorption on the anatase (101) surface is slightly weaker than those on the rutile (110) surface, which is consistent with the adsorption of H₂O on TiO₂.⁵⁰⁻⁵⁴

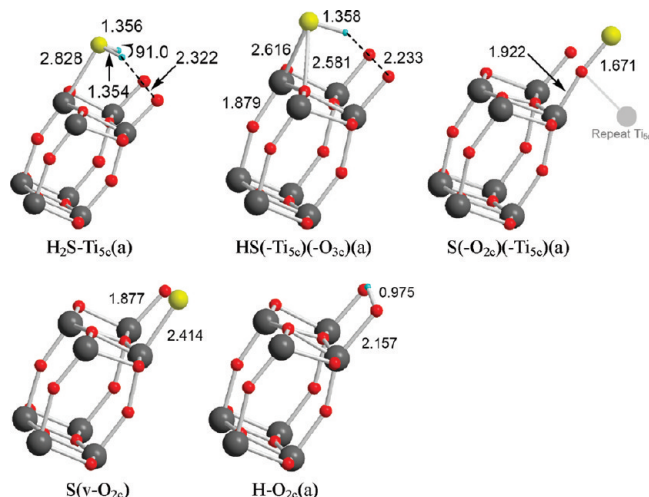


Figure 3. Optimized geometries of adsorbed H₂S and its fragments, HS, S, and H, on the TiO₂ anatase (101) surface. The bond lengths and angles are in angstroms and degrees, respectively.

HS, S, and H Adsorption. Shown in Figure 3 and Figure S2 of the Supporting Information, three types of HS adsorption configurations on the TiO₂ anatase (101) surface are found. Their adsorption energies are summarized in Table 2. Different from that on the rutile surface, the HS bound preferentially bridging at Ti_{5c} and O_{3c} sites to form HS(-Ti_{5c3c})(a) with an adsorption energy of 11.5 kcal/mol. The bond lengths of S-Ti_{5c} and S-O_{3c}, and the hydrogen bonding between H and O_{2c} are 2.616 and 2.581, and 2.233 Å, respectively. The adsorption energy of HS-Ti_{5c}(a), 11.1, is only 0.4 kcal/mol lower than that of HS(-Ti_{5c})(-O_{3c})(a), while HS-O_{2c}(a) has the lowest adsorption energy, 9.8 kcal/mol.

As shown in Figure 3 (other possible structures are depicted in Figure S2 of the Supporting Information), the S atom is favorably placed on the O_{2c} and Ti_{5c} bridging site, S(-O_{2c})(-Ti_{5c})(a). The S-(Ti_{5c})₂(a) is 13.3 kcal/mol less stable than S(-O_{2c})(-Ti_{5c})(a) due to the long Ti_{5c}-Ti_{5c} distance on the anatase surface. In addition, we also considered the adsorption of S on a reduced TiO₂ surface. As presented in Figure 3, the S atom is favorably adsorbed on an O vacant site with an absorption energy of 115.9 kcal/mol, which is as much as 26 kcal/mol higher than that on a rutile vacant site, as alluded to above. It should be noted that we were not able to locate structure S-(Ti_{5c})₂(a), O_{2c}(v) which converged to the S(v-O_{2c}) configuration because of the large Ti-Ti separation (3.824 in anatase vs 2.974 in rutile). For the reaction, TiO₂(s) → O(g) + TiO₂(with an O_{2c} vacancy), the calculated reaction energies (ΔE) are 153.5 kcal/mol for the rutile surface (agree with the results from Minot et al.⁵⁵) and 168.98 kcal/mol for the anatase surface, respectively. The higher O_{2c} vacancy formation energy on the anatase surface results in the larger adsorption energy of S(v-O_{2c}).

Similar to the rutile surface, the H atom adsorbs preferentially on the O_{2c} site, H-O_{2c}(a), with an absorption energy and O-H distance of 55.4 kcal/mol and 0.975 Å, respectively, while the adsorption energy on the Ti_{5c} site, H-Ti_{5c}(a), is only 0.3 kcal/mol.

III.1.3. HS, S, and H Co-Adsorption. As summarized in Table 3, HS-Ti_{5c}, H-O_{2c}(a), S-Ti_{5c}, H-O_{2c}, H-O_{2c}(a), and S-Ti_{5c}, H₂-O_{2c}(a) are three important adsorption structures for the H₂S reaction on both surfaces. The adsorption energies of HS, S, and H in the corresponding adsorbates are 106.2, 183.9, and 177.7 kcal/mol for the rutile surface and 101.6, 188.4, and 164.6 kcal/mol for the anatase surface, respec-

TABLE 3: Adsorption Energies (kcal/mol) for HS and S, with H Co-Adsorption on TiO₂ Rutile (110) and TiO₂ Anatase (101)

structure	HS-Ti _{5c} , H-O _{2c} (a)	S-Ti _{5c} , H-O _{2c} , H-O _{2c} (a)	S-Ti _{5c} , H ₂ -O _{2c} (a)		
	on rutile	106.2	183.9	177.7 ^a	49.4 ^b
structure	HS-(Ti _{5c}) ₂ , H-O _{2c} (a)	S-(Ti _{5c}) ₂ , H-O _{2c} , H-O _{2c} (a)	S-(Ti _{5c}) ₂ , H ₂ -O _{2c} (a)		
	on rutile	96.2	167.3	165.8 ^a	37.5 ^b
	on anatase	83.8	172.3	159.5 ^a	54.1 ^b

$$^a E_{\text{gas}} = E_{\text{S}} + E_{\text{H}} + E_{\text{H}}. \quad ^b E_{\text{gas}} = E_{\text{H}_2\text{O}}$$

tively, which are more stable than the HS-(Ti_{5c})₂, H-O_{2c}(a), S-(Ti_{5c})₂, H-O_{2c}, H-O_{2c}(a), and S-(Ti_{5c})₂, H₂-O_{2c}(a). The desorption energies for HS-Ti_{5c}, H-O_{2c}(a) → HS(g) + H-O_{2c}(a) and HS-Ti_{5c}, H-O_{2c}(a) → HO(g) + HS-Ti_{5c}(a), O_{2c}(v) were calculated to be 42.8 (46.2 for anatase) and 142.1 (118.5 for anatase) kcal/mol, respectively. In these cases, the formation of the gas-phase HS or HO is unfavorable due to their high endothermicities.

It was found that the stabilities of these structures are much larger than the sum of the individual fragments on the surface. For example, the adsorption energy of HS-Ti_{5c}, H-O_{2c}(a), 106.2 kcal/mol, is 30.2 kcal/mol larger than the sum of the individual HS-Ti_{5c}(a) (12.2 kcal/mol) and H-O_{2c}(a) (63.5 kcal/mol) on the rutile surface. The difference may result from the hydrogen bonding between the adsorbed fragments and the surface hydroxyl group. In other words, the H-O_{2c} hydroxyl group has a strong influence on the interaction between the molecule and the surface. In order to verify this phenomenon (also called the hydrogen effect), we compare the adsorption energies of H₂S-Ti_{5c}(a), HS-Ti_{5c}(a), S-(Ti_{5c})₂(a), H₂O-Ti_{5c}(a), and OH-Ti_{5c}(a) without and with hydrogen coadsorption. The surface energy is considered as TiO₂ (rutile or anatase) with a hydrogen adsorbed on it, and the adsorption energy is computed as follows:

$$E_{\text{ads}} = -(E_{\text{total}} - E_{\text{H-surf}} - E_{\text{gas}})$$

It was found that the hydrogen effect on H₂S-Ti_{5c}, H-O_{2c}(a) and H₂O-Ti_{5c}, H-O_{2c}(a) is small and negative but is large and positive on HS-Ti_{5c}, H-O_{2c}(a) and HO-Ti_{5c}, H-O_{2c}(a). The adsorption energies of H₂S-Ti_{5c}, H-O_{2c}(a) and H₂O-Ti_{5c}, H-O_{2c}(a) are 3.6 (3.2 for anatase) and 2.9 (2.3 for anatase) kcal/mol lower than the values of H₂S-Ti_{5c}(a) and H₂O-Ti_{5c}(a), respectively. In contrast, the adsorption energies of HS and HO in HS-Ti_{5c}, H-O_{2c}(a) and HO-Ti_{5c}, H-O_{2c}(a) are 30.2 and 36.6 (34.0 and 52.4 for anatase) kcal/mol larger than the values of HS-Ti_{5c}(a) and HO-Ti_{5c}(a), respectively. The HS···H distance on the rutile surface is 2.063 Å (2.218 Å on the anatase surface), and the HO···H distance on the same surface is 2.126 Å (2.597 Å on the anatase surface); hence, these distances make the formation of hydrogen bonds possible. By this way, the bonding energies of HS-Ti_{5c}, H-O_{2c}(a) and HO-Ti_{5c}, H-O_{2c}(a) are enhanced by the hydrogen coadsorption. The hydrogen coadsorption effect can play a significant role in a radical's adsorption energy, which was also supported by the observation of Lin et al.^{56–58} and Petek et al.^{59–61}

III.1.4. Bader Charge Analysis. In order to explain the hydrogen effect, we carried the Bader charge analysis for H₂S-Ti_{5c}(a) and HS-Ti_{5c}(a) with and without a hydroxyl group

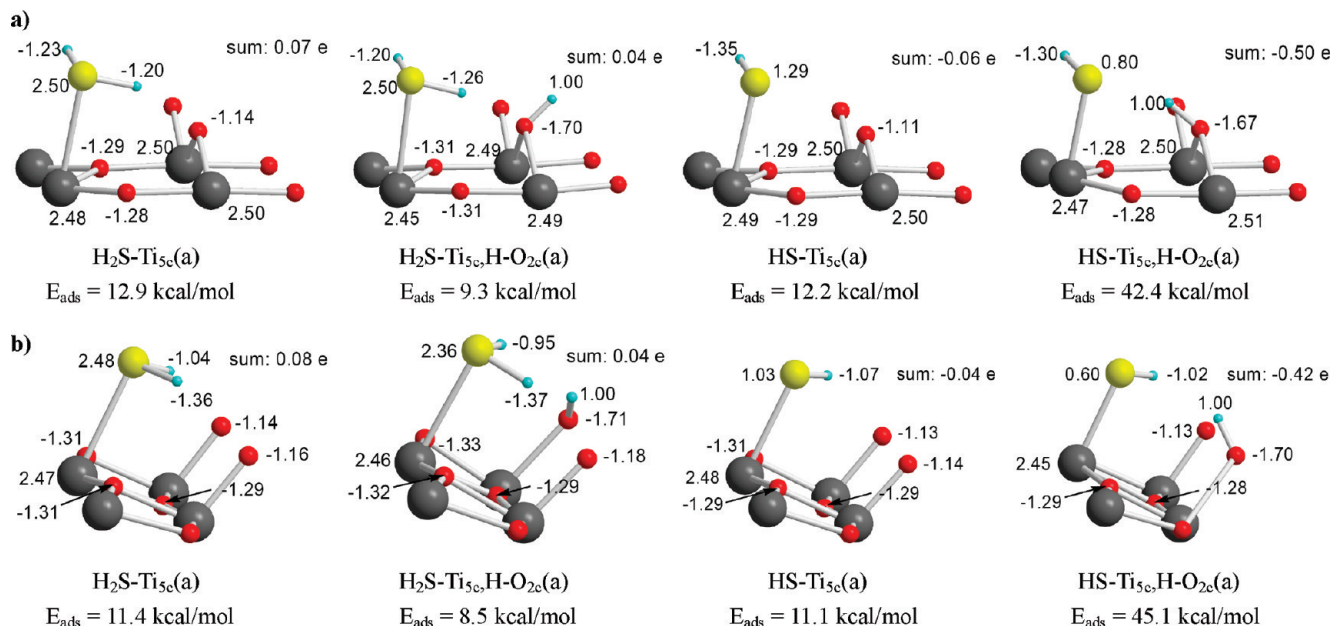


Figure 4. Bader atomic charge analyses of H₂S-Ti_{5c}(a) and HS-Ti_{5c}(a) with and without H coadsorption on the (a) TiO₂ rutile and (b) TiO₂ anatase surfaces.

on both surfaces. Shown in Figure 4, only slightly charge transfer occurred from the H₂S adsorbate of **H₂S-Ti_{5c}(a)** to the surface without hydrogen coadsorption (0.07 e for rutile and 0.08 e for anatase). Part of the exceeding electron diffuses to the bridged surface oxygen. The charge of bridged surface oxygen is 0.06 e (0.04 e/0.06e) more than that of the clean rutile (anatase) surface. When the **H₂S-Ti_{5c}(a)** coadsorbed with a hydrogen atom, the charges of H₂S adsorbate are 0.04 e for both surfaces. The difference between H₂S adsorbate on clean and hydroxyl group surfaces is nearly zero, resulting in the close adsorption energy.

Different from the H₂S adsorption on the surface, the HS adsorption receives an electron from the surface and hence has different hydrogen coadsorption behavior. The HS adsorption

gains 0.06 e (0.04 e) from the rutile (anatase) surface. The charges of the S atom with hydrogen coadsorption are 0.80 (rutile) and 0.60 e (anatase). Comparing with the S atom without H coadsorption are 1.29 (rutile) and 1.03 e (anatase). This phenomenon suggests that a H coadsorbed on the bridged surface oxygen will distribute its atomic charge into the adsorbate and stabilize the configuration with higher adsorption energy, as listed in Figure 4. In summary, the difference in the adsorption energy can be attributed to the charge transfer from surface to adsorbates.^{56–58}

III.1.5. Reaction Mechanism of H₂S-TiO₂ Rutile (110) Interactions.

To characterize the key reaction pathways of the H₂S adsorption/dissociation processes on the TiO₂ rutile (110) surface, we employed energetically the most stable configura-

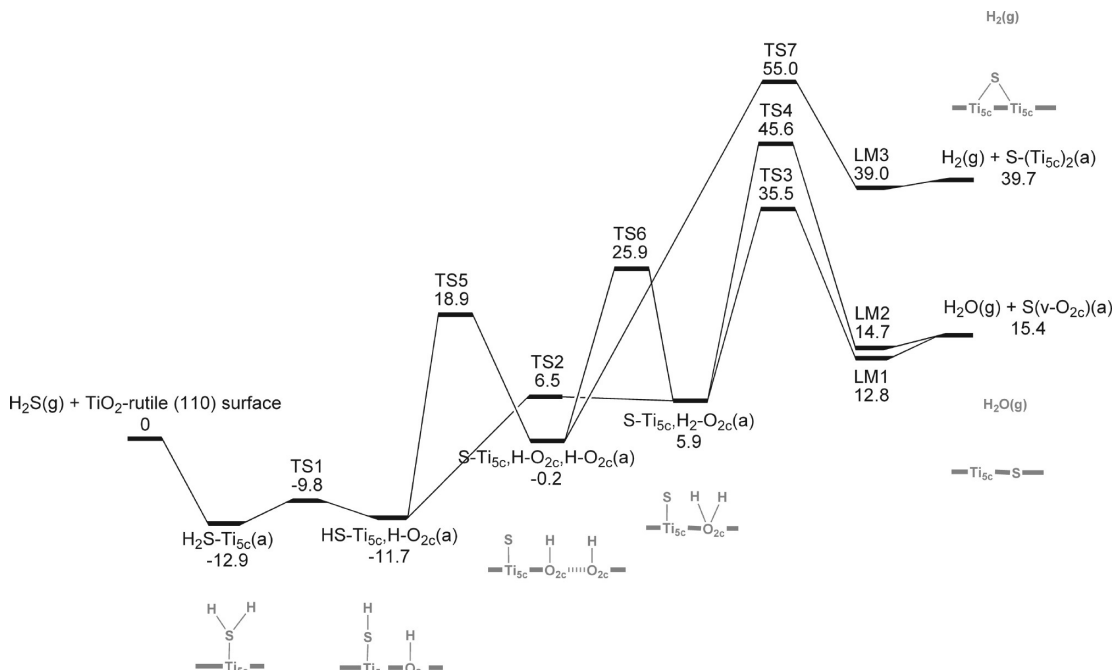
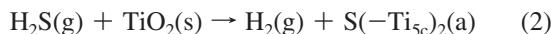


Figure 5. Schematic potential energy profiles for the reaction H₂S + TiO₂ rutile (110).

tions obtained from the H₂S, HS, and S adsorptions to map out the PES using the NEB method by connecting the local minima. Figure 5 presents the schematic potential energy profiles based on the calculations, while Figure 6 shows the optimized structures of intermediates, transition states, and products. Two possible pathways can be considered: (1) formation of H₂O(g) and an oxygen vacancy; (2) formation of H₂(g). The former represents the exchange of an oxygen on the surface with a sulfur atom:



where (s), (g), (a), and (v) denote surface, gas, adsorption, and vacancy, respectively.

Path 1. As shown in Figure 5, H₂S first adsorbs on the surface without an intrinsic transition state, producing **HS-Ti_{5c}(a)** with an exothermicity of 12.9 kcal/mol, followed by the dissociation process (H₂S → SH + H). The dissociating H atom primarily attaches to an adjacent bridging O_{2c} anion, forming an O–H bond via **TS1** with a small reaction barrier of 3.1 kcal/mol, which is close to that for H₂S dissociation on metal surfaces.^{30–32,34} The Ti–S bond length of **TS1** is shortened by approximately 0.14 Å compared to that of the molecularly adsorbed H₂S, **HS-Ti_{5c}(a)** (i.e., 2.617 and 2.757 Å, respectively). The breaking H–S and forming O–H bonds at **TS1** are 1.559 and 1.321 Å, respectively. The second dissociation step takes place by overcoming an 18.2 kcal/mol reaction barrier at **TS2**, producing H₂O-containing **S-Ti_{5c},H₂-O_{2c}(a)** with an endothermicity of 17.6 kcal/mol compared to **HS-Ti_{5c},H-O_{2c}(a)**. As shown in Figure 5, the **S-Ti_{5c},H₂-O_{2c}** adsorbate can also be formed by a stepwise pathway via the dissociation reaction (HS → S + H) by overcoming a 30.6 kcal/mol reaction barrier at **TS5**, producing **S-Ti_{5c},H₂-O_{2c},H-O_{2c}(a)** with an endothermicity of 11.5 kcal/mol compared to **HS-(Ti_{5c})₂,H-O_{2c}(a)**. At **TS5**, the breaking S–H and forming O–H bonds are 1.609 and 2.066 Å, respectively, while the Ti–S bond length is 2.411 Å. The two H–O_{2c} species of the **S-Ti_{5c},H₂-O_{2c},H-O_{2c}(a)** intermediate can undergo H-migration via **TS6** with a reaction barrier of 26.1 kcal/mol, leading to the H₂O-containing **S-Ti_{5c},H₂-O_{2c}(a)** intermediate with an endothermicity of 6.1 kcal/mol. The forming and breaking O–H bonds in **TS6** are 1.544 and 1.076 Å, respectively. The stepwise pathway is less favorable due to the higher reaction barriers (at **TS5** and **TS6**).

Due to the formation of an H₂O species along with the reduction of Ti⁴⁺ to Ti³⁺, an oxygen vacancy is generated, the S atom can move into the O vacant site along with the H₂O dissociation to form **LM1** and **LM2** with the reaction barriers of 29.6 and 39.7 kcal/mol followed by H₂O desorption from **LM1** and **LM2**, which are weakly physisorbed H₂O species with small adsorption energies of 2.6 and 0.7 kcal/mol, respectively. The reaction energy of **S-Ti_{5c},H₂-O_{2c}(a)** → H₂O(g) + S(v-O_{2c}) was calculated to be 9.5 kcal/mol, which is much smaller than that of **H₂-O_{2c}(a)** → H₂O(g) + O_{2c}(v), 23.5 kcal/mol, indicating that sulfur can lower the desorption energy of H₂O from the surface.

Path 2. As presented in Figure 5, the OH-containing **S-Ti_{5c},H₂-O_{2c},H-O_{2c}(a)** intermediate can undergo the dehydrogenation process, giving **LM3** via **TS7** with the highest reaction barrier of 55.2 kcal/mol, suggesting that the H₂-elimination pathway is less favorable than other processes. The weakly bound H₂ species of **LM3** can barrierlessly desorb to produce **H₂(g)** + **S-(Ti_{5c})₂(a)** with an overall endothermicity of 39.7 kcal/mol.

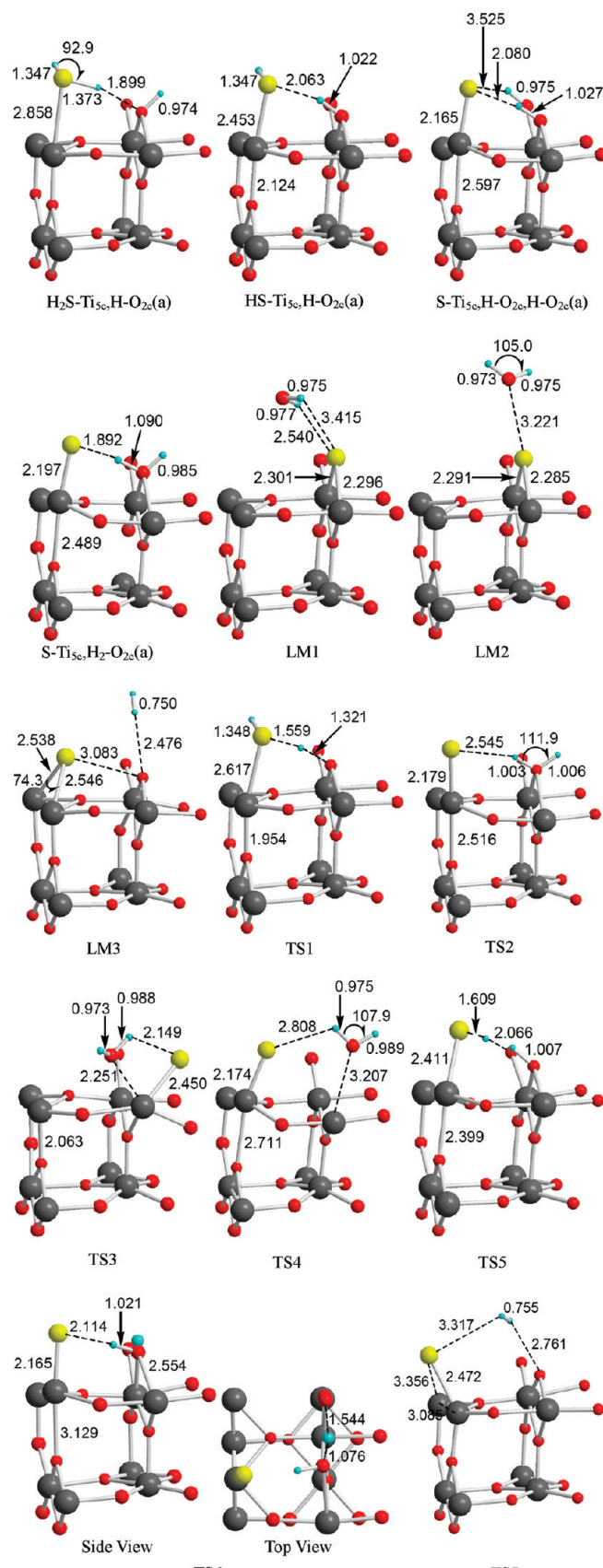


Figure 6. Optimized geometries of intermediates, transition states, and products for the H₂S + TiO₂ rutile (110) reaction.

Kinetics. On the basis of the aforementioned PES for the reaction of H₂S on TiO₂ rutile (110), as shown in Figure 5, we have carried out microcanonical Rice–Ramsperger–Kassel–

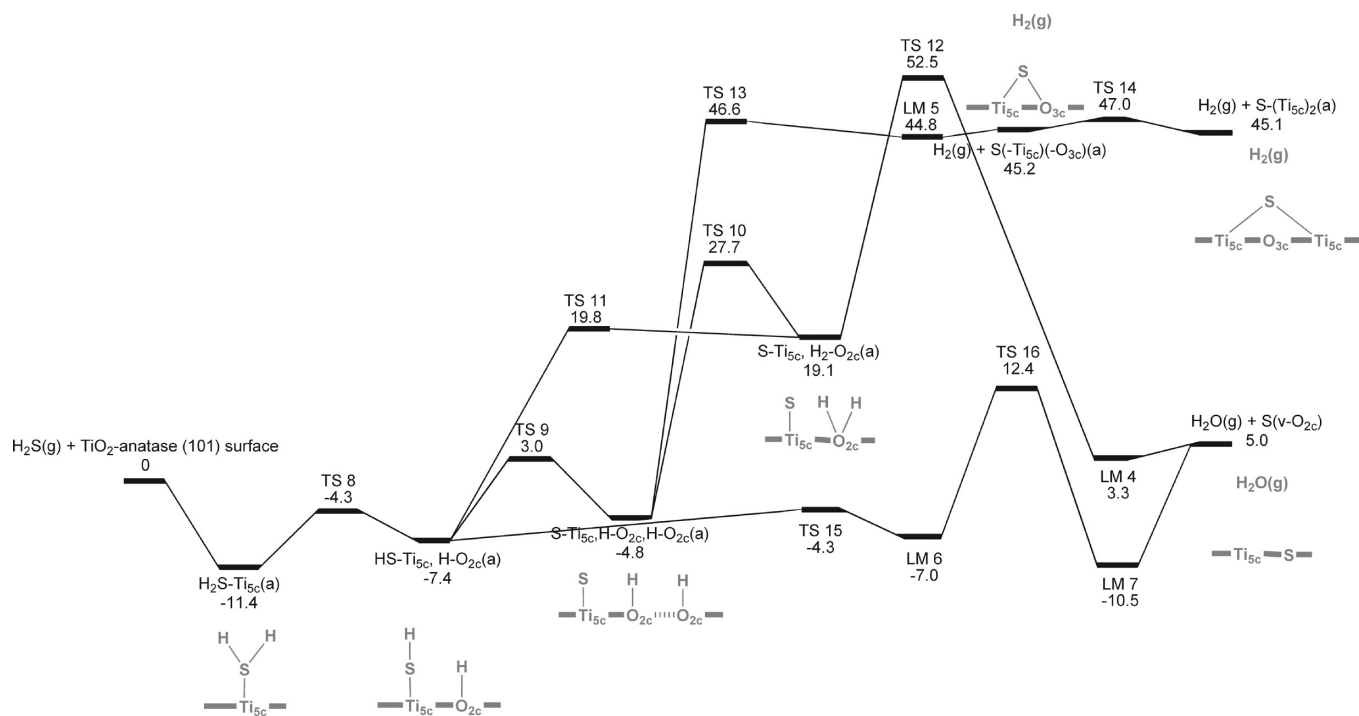
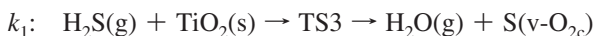


Figure 7. Schematic potential energy profiles for the reaction H₂S + TiO₂ anatase (101).

Marcus (RRKM) theory calculations using the ChemRate program⁴⁵ for the following two channels:



for which the rate constants, k_1 and k_2 , are controlled by the well-defined TS3 and TS7, respectively. Under the condition for the S-for-O endothermic replacement process which is expected to occur during metal-sulfide deposition processes, for example, the precursor reactions with energies lower than the barrier at TS3 are essentially in equilibrium. The predicted rate constants (in molecular units, cm³/s) in the temperature range 300–2000 K can be represented by

$$k_1 = 1.38 \times 10^{-22} T^{2.40} \exp(-33.94 \text{ kcal mol}^{-1}/RT)$$

$$k_2 = 9.40 \times 10^{-26} T^{3.71} \exp(-53.60 \text{ kcal mol}^{-1}/RT)$$

Here, the rate constants for these dissociative adsorption processes are defined by⁶² the equation $d[X]_{\text{surf}}/dt = k(\theta/A_s)[X]_{\text{g}}$, which has units of flux, molecules cm⁻² s⁻¹. In this equation, θ , A_s , and $[X]_{\text{g}}$ represent the fraction of available surface sites, the surface area, and the concentration of the H₂S gas in molecules/cm³, respectively. The value of k_1 is 2×10^{15} times higher than that of k_2 at 300 K, as one would expect from the large barrier difference. These results may be employed for simulation of metal sulfide thin-film deposition on titania as referred to above.

III.1.6. Reaction Mechanism of H₂S-TiO₂ Anatase (110) Interactions. Similar to the rutile surface, two possible pathways can be considered: (1) formation of H₂O(g) and an oxygen vacancy; (2) formation of H₂(g). Figure 7 presents the schematic potential energy profiles based on the calculations, while Figure

8 shows the optimized structures of intermediates, transition states, and products.

Path 1. As shown in Figure 7, H₂S first adsorbs on the surface without an intrinsic transition state, producing H₂S-Ti_{5c}(a) with an exothermicity of 11.4 kcal/mol, followed by the dissociation process (H₂S → SH + H). The dissociating H atom primarily attaches to an adjacent bridging O_{2c} anion, forming an O–H bond via TS8 with a reaction barrier of 7.1 kcal/mol. The Ti–S bond length of TS8 is shortened by approximately 0.18 Å compared to that of the molecularly adsorbed H₂S, H₂S-Ti_{5c}(a) (i.e., 2.644 and 2.828 Å, respectively). The breaking H–S and forming O–H bonds at TS8 are 1.603 and 1.318 Å, respectively.

Starting from HS-Ti_{5c}, H-O_{2c}(a), as shown in Figure 7, the H₂O-containing S-Ti_{5c}, H₂-O_{2c}(a) can be formed via two mechanisms: (1) overcoming a 27.2 kcal/mol energy barrier at TS11; (2) a stepwise pathway via the dissociation reaction (HS → S + H) by overcoming a 10.4 kcal/mol reaction barrier at TS9, producing S-Ti_{5c}, H₂-O_{2c}, H-O_{2c}(a) with an endothermicity of 2.6 kcal/mol compared to HS-Ti_{5c}, H-O_{2c}(a). Then, one of the two H–O_{2c} species of the S-Ti_{5c}, H₂-O_{2c}, H-O_{2c}(a) intermediate can undergo H-migration via TS10 with a reaction barrier of 32.5 kcal/mol, leading to the H₂O-containing S-Ti_{5c}, H₂-O_{2c}(a) intermediate with an endothermicity of 23.9 kcal/mol.

LM4, which is a weakly physisorbed H₂O species with an oxygen vacancy on the surface, with a small adsorption energy of 1.7 kcal/mol is formed by passing TS12 with a high energy barrier of 33.4 kcal/mol. The weakly physisorbed H₂O species can easily be removed from LM4, forming the S-doped TiO₂ surface. The reaction energy of S-Ti_{5c}, H₂-O_{2c}(a) → H₂O(g) + S(v-O_{2c}) was calculated to be -14.1 kcal/mol, which is smaller than that of H₂-O_{2c}(a) → H₂O(g) + O_{2c}(v), 24.4 kcal/mol, indicating again that sulfur can lower the desorption energy of H₂O from the TiO₂ surface. It is worth noting that the OH radical in HS-Ti_{5c}, H-O_{2c}(a) can easily rotate to another direction to form LM6, by overcom-

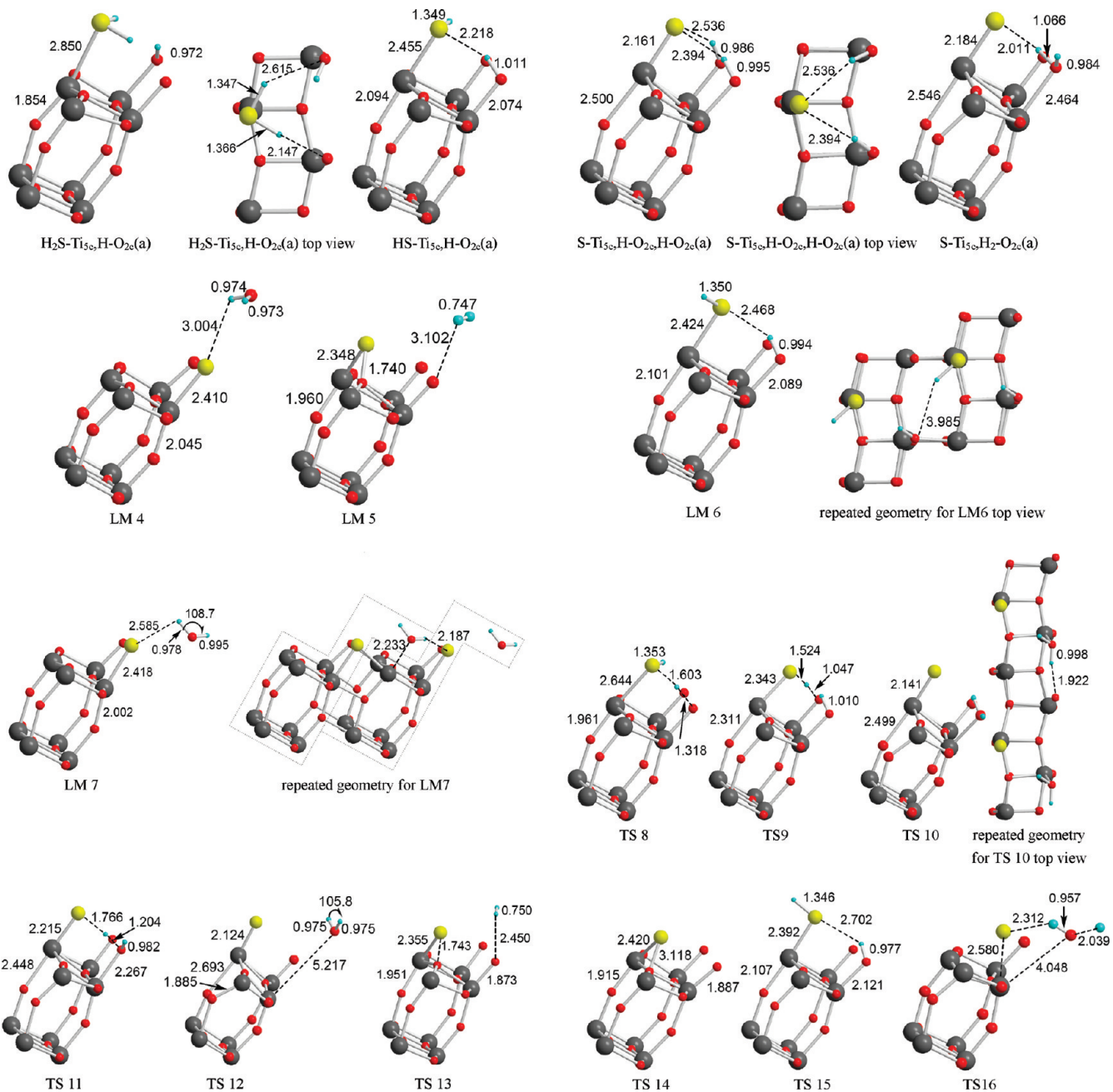


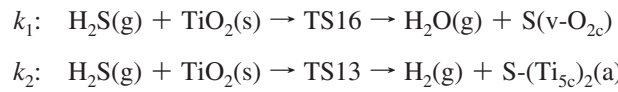
Figure 8. Optimized geometries of intermediates, transition states, and products for the $\text{H}_2\text{S} + \text{TiO}_2$ anatase (101) reaction.

ing a 3.1 kcal/mol energy barrier, **TS15**. Then, the H atom HS can move to OH, forming the H_2O -containing **LM7** by overcoming a barrier of 19.4 kcal/mol at **TS16** accompanying the incorporation of a S atom into the O_{2c} vacancy site. **LM7**, which cannot be found on the rutile surface, is more stable than the similar H_2O containing structure, **LM1**, **LM2**, and **LM4**, because of the formation of an $\text{O}-\text{Ti}_{5c}$ bond (2.233 Å) and hydrogen bond (2.187 Å). This process of $\text{H}_2\text{S(g)} + \text{TiO}_2(\text{s}) \rightarrow \text{TS3} \rightarrow \text{H}_2\text{O(g)} + \text{S(v-O}_{2c}\text{)}$ is more favorable to occur compared with that on the rutile surface due to the lower barrier and lesser endothermicity on the anatase surface.

Path 2. As presented in Figure 7, the OH-containing **S-Ti_{5c},H-O_{2c},H-O_{2c}(a)** intermediate can undergo the dehydrogenation process, giving **LM5** via **TS13** with a reaction barrier of 46.6 kcal/mol. The weakly bound H_2 species of **LM5** can barrierlessly desorb to produce $\text{H}_2(\text{g}) +$

S-(Ti_{5c})(-O_{3c})(a) with a small endothermicity of 0.4 kcal/mol. The higher barrier and endothermicity of the $\text{H}_2(\text{g})$ formation process compared with the $\text{H}_2\text{O(g)}$ formation process suggest that the H_2 -elimination pathway is less favorable than other processes.

Kinetics. On the basis of the aforementioned PES for the reaction of H_2S on TiO_2 anatase (101), as shown in Figure 7, we have carried out RRKM theory calculations using the ChemRate program⁴⁵ for the following two channels:



for which the rate constants, k_1 and k_2 , are controlled effectively by the well-defined **TS16** and **TS13**, respectively. The predicted

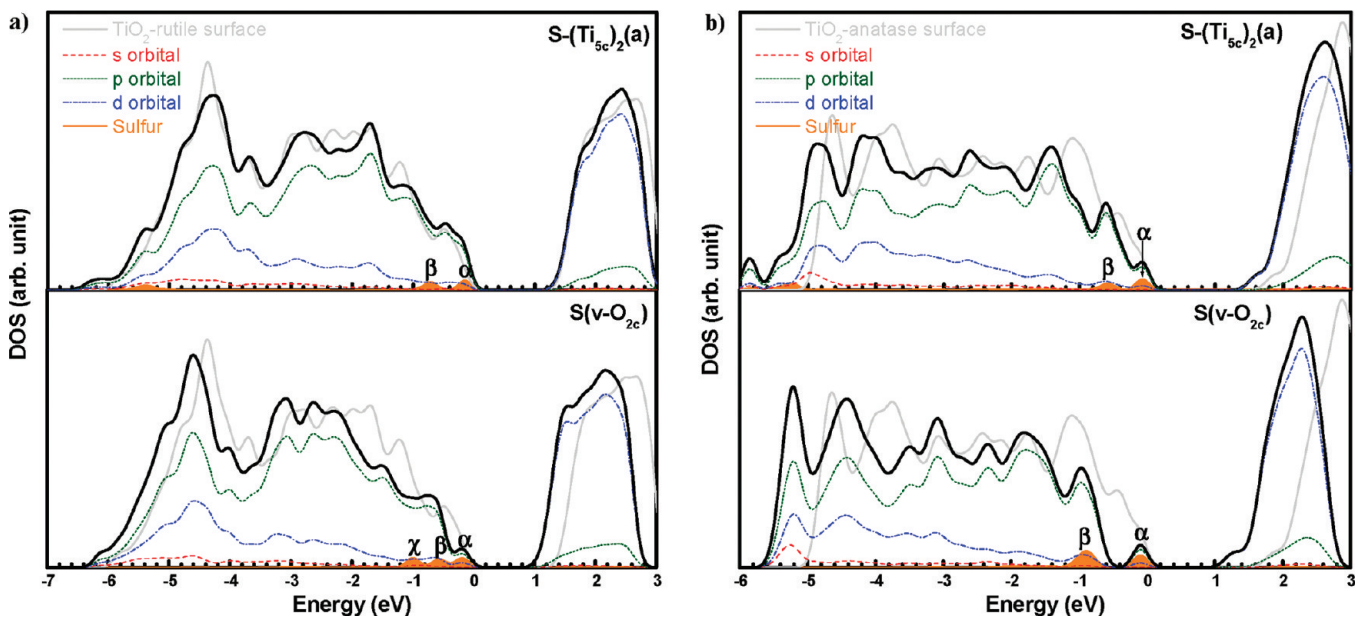


Figure 9. Total density of states and its projected density of states of S-(Ti_{5c})₂ and S(v-O_{2c}) on the (a) TiO₂ rutile and (b) TiO₂ anatase surfaces.

rate constants (in molecular units, cm³/s) in the temperature range 300–2000 K can be represented by

$$k_1 = 3.66 \times 10^{-23} T^{2.95} \exp(-11.38 \text{ kcal mol}^{-1}/RT)$$

$$k_2 = 7.87 \times 10^{-25} T^{3.79} \exp(-45.84 \text{ kcal mol}^{-1}/RT)$$

The value of k_1 is 3×10^{24} times greater than that of k_2 at 300 K because of the large barrier difference.

III.1.7. Electronic Structures of S-Doped TiO₂. The total density of state and project density of state are used to analyze the band gap change with a Gaussian smearing factor of 0.1 eV. Figure 9 shows the DOS (density of state) and PDOS (projected density of state) of S-doped TiO₂, S-(Ti_{5c})₂(a), and S(v-O_{2c}). In S-(Ti_{5c})₂(a), the S 3p state located at the upper part of the valence band is divided into two parts: 3P_π state in position α and 3P_σ state in position β. The S 3P_π state mixed with O_{3c} 2p_π and Ti_{5c} 3d is around 0.13 eV (0.48 eV) above the valence band of the clean rutile (anatase) surface, and hence, the band gap of the TiO₂ surface is reduced by the sulfur doping. The band gap changes of S-(Ti_{5c})₂(a) have a similar behavior for the two TiO₂ surfaces, but it is very different for S(v-O_{2c}). The S 3p state of S(v-O_{2c}) on rutile TiO₂ located at the upper part of the valence band is divided into three parts: 3p_π state in position α and χ and 3p_σ states in position β. The S 3p_π state in position α mixed with Ti 3d (mainly e_g state) is 0.22 eV above the valence band of the clean rutile TiO₂ surface, and the band gap of the surface is narrowed by the doped S 3p_π state. The sulfur of S(v-O_{2c}) on the rutile surface bonds with two Ti_{5c} sites, and the two Ti_{5c} 3d states have the same contribution on the DOS. Different from the rutile surface, the sulfur of S(v-O_{2c}) on the anatase surface bonds with one Ti_{5c} site and one Ti_{6c} site on the surface. The S 3p state close to the valence band is divided into two parts: S 3p_σ in position α and two very close 3p_π (-0.85 and -0.97 eV) in position β. The S 3p_σ mixes with the two Ti t_{2g} states, and the ratio of the t_{2g} state from Ti_{5c} and from Ti_{6c} is around 4:1. It means that the Ti_{5c} site is contributed to the TiO₂ band gap modification more. The S 3p_σ state is 0.53 eV above the valence band of the clean

anatase surface. In addition, the Fermi level is also moved by the S on the surface. The Fermi levels of S-(Ti_{5c})₂(a) and S(v-O_{2c}) are 0.28 eV (0.55 eV) and 0.42 eV (0.63 eV) lower than those of the pure rutile (anatase) surface.

In summary, the band gap reduction of S(v-O_{2c}) is more significant than that of S-(Ti_{5c})₂(a), while S-doped anatase is more significant than S-doped rutile TiO₂. Thereupon, the S(v-O_{2c}) on the anatase surface shows the best application of band gap modification. The sulfur doping results in the red shift of UV adsorption for TiO₂, but only the S(v-O_{2c}) on the anatase surface gives the probability of visible light adsorption. These results are also observed in experimental works.^{23,24,63,64}

IV. Conclusion

The interaction of H₂S with the TiO₂ surface has been examined by periodic DFT calculations. Three sulfur-containing species (H₂S, HS, and atomic S) were initially employed to locate reasonable intermediates. It was found that H₂S, HS, S, and H preferentially adsorb at the Ti_{5c}, O_{2c}, (Ti_{5c})₂, and O_{2c} sites, respectively, with adsorption energies of 12.9, 18.7, 38.6, and 63.5 kcal/mol on the rutile (110) surface but at the Ti_{5c}, (Ti_{5c})₂, (-O_{2c})-(Ti_{5c}), and O_{2c} sites, respectively, with adsorption energies of 11.4, 11.5, 46.5, and 55.4 kcal/mol on the anatase (101) surface. Potential energy surfaces for the reactions of H₂S with the two TiO₂ surfaces have been constructed. According to our calculations, there are two possible products; one is H₂O(g) + S(v-O_{2c}), and the other one is H₂(g) + S-(Ti_{5c})₂(a). The formation of surface sulfur species, S(v-O_{2c}), by a complete O ↔ S exchange at the rutile (110) surface requires a barrier of 35.5 kcal/mol with an endothermicity of 15.4 kcal/mol; it may be the most possible reaction mechanism for the thermal reaction of H₂S with the TiO₂ surface. The O ↔ S exchange product, S(v-O_{2c}), is more favorably formed on the anatase (101) surface compared with that on the rutile surface due to its lower barrier (12.4 kcal/mol) and lesser endothermicity (5.0 kcal/mol) on the anatase surface. We also have predicted the rate constants for the dehydration and dehydrogenation of H₂S on the TiO₂ surface. The results of this study may be further utilized, for example, for the deposition of an InS_x thin film on titania in the near future.

Acknowledgment. The authors are grateful to Taiwan's National Center for High-performance Computing for the CPU and to Institute of Nuclear Energy Research, Atomic Energy Council, Taiwan, for the research support, and would also like to acknowledge partial support from the ATU Plan of MOE, Taiwan. M.C.L. also wants to acknowledge Taiwan Semiconductor Manufacturing Co. for the TSMC Distinguished Professorship and Taiwan National Science Council for the Distinguished Visiting Professorship at the Center for Interdisciplinary Molecular Science, National Chiao Tung University, Hsinchu, Taiwan.

Supporting Information Available: Other possible optimized geometries for H₂S, HS, S, and H adsorption on the rutile and antase surfaces. This material is available free of charge via the Internet at <http://pubs.acs.org>.

References and Notes

- (1) Hadjivanov, K. I.; Klissurski, D. G. *Chem. Soc. Rev.* **1996**, 25, 61.
- (2) Linsebigler, A. L.; Lu, G.; Yates, J. T. *Chem. Rev.* **1995**, 95, 735.
- (3) Fujishima, A.; Honda, K. *Nature* **1972**, 238, 37.
- (4) Gratzel, M. *Nature* **2001**, 414, 338.
- (5) Asahi, R.; Morikawa, T.; Ohwaki, T.; Aoki, K.; Taga, Y. *Science* **2001**, 293, 269.
- (6) Wang, J.-H.; Lin, M. C.; Sun, Y.-C. *J. Phys. Chem. B* **2005**, 109, 5133.
- (7) Rego, L. G. C.; Batista, V. S. *J. Am. Chem. Soc.* **2003**, 125, 7989.
- (8) Duncan, W. R.; Stier, W. M.; Prezhdo, O. V. *J. Am. Chem. Soc.* **2005**, 127, 7941.
- (9) Harris, L. A.; Quong, A. A. *Phys. Rev. Lett.* **2004**, 93, 086105.
- (10) Fahmi, A.; Ahdjoudj, J.; Minot, C. *Catal. Today* **1996**, 352, 529.
- (11) Li, D.; Haneda, H.; Hishita, S.; Ohashi, N. *Chem. Mater.* **2005**, 17, 2596.
- (12) Zhao, W.; Ma, W.; Chen, C.; Zhao, J.; Shuai, Z. *J. Am. Chem. Soc.* **2004**, 126, 4782.
- (13) Khan, S. U. M.; Al-Shahry, M.; Ingler, W. B., Jr. *Science* **2002**, 297, 2243.
- (14) Lin, Z.; Orlov, A.; Lambert, R. M.; Payne, M. C. *J. Phys. Chem. B* **2005**, 109, 20948.
- (15) Valentini, C. D.; Pacchioni, G.; Selloni, A.; Livraghi, S.; Giamello, E. *J. Phys. Chem. B* **2005**, 109, 11414.
- (16) Sathish, M.; Viswanathan, B.; Viswanath, R. P.; Gopinath, C. S. *Chem. Mater.* **2005**, 17, 6349.
- (17) Diwald, O.; Thompson, T. L.; Goralski, E. G.; Walck, S. D.; John T. Yates, J. *J. Phys. Chem. B* **2004**, 108, 52.
- (18) Sakthivel, S.; Kisch, H. *ChemPhysChem* **2003**, 4, 487.
- (19) Khan, S. U. M.; Al-Shahry, M.; Ingler, W. B., Jr. *Science* **2002**, 297, 2243.
- (20) Irie, H.; Watanabe, Y.; Hashimoto, K. *J. Phys. Chem. B* **2003**, 107, 5483.
- (21) Burda, C.; Lou, Y.; Chen, X.; Samia, A. C. S.; Stout, J.; Gole, J. L. *Nano Lett.* **2003**, 3, 1049.
- (22) Tian, F.; Liu, C. *J. Phys. Chem. B* **2006**, 110, 17866.
- (23) Smith, M. F.; Setwong, K.; Tongpool, R.; Onkaw, D.; Na-phattalung, S.; Limpijumnong, S.; Rujirawat, S. *Appl. Phys. Lett.* **2007**, 91, 142107.
- (24) Chen, Y.; Jiang, Y.; Li, W.; Jin, R.; Tang, S.; Hu, W. *Catal. Today* **1999**, 50, 39.
- (25) Fahmi, A.; Ahdjoudj, J.; Minot, C. *Surf. Sci.* **1996**, 352–354, 529.
- (26) Rodriguez, J. A.; Hrbek, J.; Chang, Z.; Dvorak, J.; Jirsak, T. *Phys. Rev. B* **2002**, 65, 235414.
- (27) Ziolek, M.; Kujawa, J.; Saur, O.; Lavalle, J. C. *J. Mol. Catal. A* **1995**, 97, 49.
- (28) Rodriguez, J. A.; Chaturvedi, S.; Kuhn, M.; Hrbek, J. *J. Phys. Chem. B* **1998**, 102, 5511.
- (29) Chen, H.-T.; Choi, Y. M.; Liu, M.; Lin, M. C. *J. Phys. Chem. C* **2007**, 111, 11117.
- (30) Jiang, D. E.; Carter, E. A. *J. Phys. Chem. B* **2004**, 108, 19140.
- (31) Jiang, D. E.; Carter, E. A. *Surf. Sci.* **2005**, 583, 60.
- (32) Albenze, E. J.; Shamsi, A. *Surf. Sci.* **2006**, 600, 3202.
- (33) Qin, C.; Whitten, J. L. *Surf. Sci.* **2005**, 588, 83.
- (34) Choi, Y. M.; Compson, C.; Lin, M. C.; Liu, M. *Chem. Phys. Lett.* **2006**, 421, 179.
- (35) Burnside, S. D.; Shklover, V.; Barbe, C.; Comte, P.; Arendse, F.; Brooks, K.; Gratzel, M. *Chem. Mater.* **1998**, 10, 2419.
- (36) Labat, F.; Baranek, P.; Adamo, C. *J. Chem. Theory Comput.* **2008**, 4, 341.
- (37) Kresse, G.; Furthmuller, J. *J. Comput. Mater. Sci.* **1996**, 6, 15.
- (38) Kresse, G.; Furthmuller, J. *Phys. Rev. B* **1996**, 54, 11169.
- (39) Blochl, P. *Phys. Rev. B* **1994**, 17, 953.
- (40) Perdew, J. P.; Wang, Y. *Phys. Rev. B* **1992**, 45, 13244.
- (41) Perdew, J. P.; Chevary, J. A.; Vosko, S. H.; Jackson, K. A.; Penderson, M. R.; Singh, D. J.; Fiolhais, C. *Phys. Rev. B* **1992**, 46, 6671.
- (42) Herman, G. S.; Dohnalek, Z.; Ruzycki, N.; Diebold, U. *J. Phys. Chem. B* **2003**, 107, 2788.
- (43) Henkelman, G.; Uberuaga, B. P.; Jönsson, H. *J. Chem. Phys.* **2000**, 113, 9901.
- (44) Mills, G.; Jonsson, H.; Schenter, G. K. *Surf. Sci.* **1995**, 324, 305.
- (45) Mokrishi, W. B., V.; Tsang, W.; Zachariah, M.; Knyazev, V. *ChemRate*, version 1.5.2; National Institute of Standards and Technology: Gaithersburg, MD, 2006.
- (46) Henkelman, G.; Arnaldsson, A.; Jonsson, H. *Comput. Mater.* **2006**, 36, 354.
- (47) Burdett, J. K.; Hughbanks, T.; Miller, G. J.; Richardson, J. W.; Smith, J. V. *J. Am. Chem. Soc.* **1987**, 109, 3639.
- (48) Howard, C. J.; Sabine, T. M.; Dickson, F. *Acta Crystallogr.* **1991**, 47, 462.
- (49) Shiell, R. C.; Hu, X. K.; Hu, Q. J.; Hepburn, J. W. *J. Phys. Chem. A* **2000**, 104, 4339.
- (50) Tilcock, A.; Selloni, A. *Langmuir* **2004**, 20, 8379.
- (51) Herman, C. S.; Dohnalek, Z.; Ruzycki, N.; U, D. *J. Phys. Chem. B* **2003**, 107, 2788.
- (52) Harris, L. A.; Quong, A. A. *Phys. Rev. Lett.* **2004**, 93, 086105.
- (53) Lindan, P. J. D.; Harrison, N. M. *Phys. Rev. Lett.* **1998**, 80, 762.
- (54) Hugenschmidt, M. B.; Gamble, L.; Campbell, C. T. *Surf. Sci.* **1994**, 302, 329.
- (55) Bouzoubaa, A.; Markovits, A.; Calatayud, M.; Minot, C. *Phys. Rev. B* **2005**, 583, 107.
- (56) Chang, C.-Y.; Chen, H.-T.; Lin, M. C. *J. Phys. Chem. C* **2009**, 113, 6140.
- (57) Raghunath, P.; Lin, M. C. *J. Phys. Chem. C* **2008**, 112, 8276.
- (58) Raghunath, P.; Lin, M. C. *J. Phys. Chem. C* **2009**, 113, 3751.
- (59) Zhao, J.; Li, B.; Jordan, K. D.; Yang, J.; Petek, H. *Phys. Rev. B* **2006**, 73, 195309.
- (60) Onda, K.; Li, B.; Zhao, J.; Jordan, K. D.; Yang, J.; Petek, H. *Science* **2005**, 308, 1154.
- (61) Liu, L. M.; Mcallister, B.; Ye, H. Q.; Hu, P. *J. Am. Chem. Soc.* **2006**, 128, 4017.
- (62) Rettner, C. T.; Ashfold, M. N. R. *Dynamics of Gas-Surface Interaction*; Springer-Verlag: Berlin, 1991.
- (63) Umebayashi, T.; Yamaki, T.; Itoh, H.; Asai, K. *Appl. Phys. Lett.* **2002**, 81, 454.
- (64) Umebayashi, T.; Yamaki, T.; Tanaka, S.; Asai, K. *Chem. Lett.* **2003**, 32, 330.